Removal of copper from cattle footbath wastewater with layered double hydroxide adsorbents as a route to antimicrobial resistance mitigation on dairy farms

Orla Williams [a], Ian Clark [a], Rachel L. Gomes [a,*], Tania Perehinec [b], Jon L. Hobman [b], Dov J. Stekel [b], Robert Hyde [c], Chris Dodds [a], Edward Lester [a]

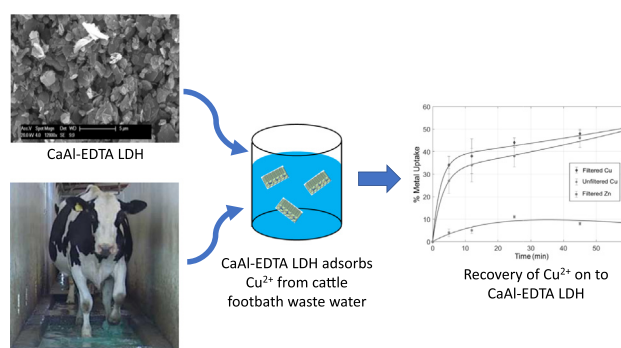[a] Faculty of Engineering, University of Nottingham, University Park, Nottingham NG7 2RD, UK
[b] School of Biosciences, University of Nottingham, Sutton Bonington Campus, Leicestershire LE12 5RD, UK
[c] School of Veterinary Medicine and Science, University of Nottingham, Sutton Bonington Campus, Leicestershire LE12 5RD, UK

HIGHLIGHTS

- Copper and zinc are routinely used as antimicrobials in cattle footbaths.
- Potential antimicrobial resistance (AMR) mitigation method examined.
- Layered Double Hydroxides successfully removed copper and zinc from cattle footbath.
- The kinetics of all sorption systems fitted well to a pseudo second-order model.
- Novel and economically positive way to remove potential source of AMR established.

GRAPHICAL ABSTRACT

CaAl-EDTA LDH

CaAl-EDTA LDH adsorbs Cu²⁺ from cattle footbath waste water

Recovery of Cu²⁺ on to CaAl-EDTA LDH

ARTICLE INFO

ABSTRACT

Copper and zinc are routinely used in livestock antimicrobial footbaths in commercial farming. The footbath mix is a cost to farmers, and the disposal of spent footbath into slurry tanks leads to soil contamination, as well as the potential for antimicrobial metal resistance and co-selection. This study assesses the potential to mitigate a source of antimicrobial metal resistance in slurry tanks while recovering copper and zinc from spent cattle footbaths. This is the first study in literature to investigate the potential of recovering copper from cattle footbath solutions via any method. The sorbent, Ca_2Al-EDTA Layered Double Hydroxides (LDH), were used to remove Cu^{2+} from a $Cu_2SO_4 \cdot 5H_2O$ solution at different temperatures. The maximum Cu^{2+} uptake from the $Cu_2SO_4 \cdot 5H_2O$ solution was 568 ± 88 mg g^{-1}. Faster and higher equilibrium uptake was achieved by increasing the temperature of the solution. The sorbent was found to be effective in removing copper and zinc from a commercially available cattle footbath solution (filtered footbath solution Cu^{2+} uptake 283 ± 11.05 mg g^{-1}, Zn^{2+} uptake 60 ± 0.05 mg g^{-1}). Thus, this study demonstrates the opportunity for a completely novel and potentially economically beneficial method of mitigating antimicrobial resistance in agriculture and the environment, while also providing a new valuable copper and zinc waste stream for secondary metal production.

© 2018 Published by Elsevier B.V.

* Corresponding author.
E-mail address: Rachel.gomes@nottingham.ac.uk (R.L. Gomes).

1. Introduction

Agricultural systems have been reported to be one of the key routes for the development and spread of antimicrobial resistance (AMR) within the environment (Department of Health, 2014). Heavy metals such as copper and zinc, have a long history of being used as antimicrobials in medicine and agriculture (Hobman and Crossman, 2015). Footbaths containing up to 10% copper and zinc sulphate are used on dairy farms for mass preventative treatment of cattle lameness caused by bacterial infections such as digital dermatitis (Holzhauer et al., 2012). After use, these footbath solutions are usually disposed of in slurry tanks, where they can reside for up to several months, before commonly being spread on to the land (Laven and Logue, 2006). Despite metals being resident in slurry tanks, heavy metals are not subject to reduction in this medium (Baker et al., 2016; Yu et al., 2017). If heavy metals are allowed to accumulate in the environment, they could co-select antibiotic resistance and metal resistance in microorganisms (Guo et al., 2018; Seiler and Berendonk, 2012), and increase levels of copper and zinc on farmland where slurry is spread. Thus, eliminating the disposal of waste cattle footbath into slurry tanks could potentially not only provide a plentiful source of recoverable copper and zinc, but also reduce the environmental impact of spreading slurry while mitigating this potential source of AMR co-selection and metal resistance (Department of Health, 2014; Hobman and Crossman, 2015).

AMR has been declared "a major global threat to public health" by the World Health Organisation, and the estimated associated economic costs by 2050 could be as high as 100 trillion US Dollars (Hobman, 2016). Antibiotic resistance can be acquired by bacteria via mutations of target proteins and/or regulatory genes or motifs, or through acquisition of resistance genes from other microorganisms (Pal et al., 2017). Metal resistance is a common phenotype in many microorganisms that are exposed to metals in their habitats (Hobman and Crossman, 2015), and antibiotic and metal resistance genes are frequently co-located on mobile genetic elements, providing the potential for co-selection. Copper has traditionally been used in agriculture, and is increasingly being utilised in areas such as hospitals as an antimicrobial material due to its broad-spectrum activity against bacteria, viruses, yeasts and fungi (Schmidt et al., 2016). In addition to its use in cattle footbaths and as a fungicide, copper is also added to animal feed to promote growth due to its influence on the gut microbiota (Hobman and Crossman, 2015). However, the use of copper in animal feed has been associated with increased levels of AMR in microbial populations from farm animals and animal faeces (Zhu et al., 2013). Although AMR has traditionally been viewed as a clinical issue, the propagation of resistance to antimicrobials is actually an environmental challenge, and both human and agricultural uses of antimicrobials have contributed to this situation (Department of Health, 2014; Summers, 2006). The influence of conditions where bacteria are stored for long periods in environments such as slurry tanks, which contain biologically relevant levels of antibiotics, and metals such as copper are crucial in understanding and combating these multi-drug resistance and transmission phenomena (Hobman and Crossman, 2015). Thus, removing AMR co-selection drivers such as metals in cattle footbaths in slurry tanks can only be seen as a positive step in the fight against AMR propagation.

Waste cattle footbaths could potentially be a significant source of recycled copper and zinc. A typical cattle footbath contains 25 kg of footbath mix and 200 L of water per 50–200 cows. Given that there are approximately 1.9 million dairy cattle in the UK (Bate, 2016), potentially up to 400 million L of footbath is being disposed every year through slurry tanks. Despite rising demand for copper, the environmental and economic impacts of increased production and declining ore grades means that copper mining is becoming more prohibitive and expensive (Northey et al., 2014). The main challenge of future raw material extraction is the escalating unit energy costs of production (Frenzel et al., 2017), and secondary production of copper requires ≤85% less energy than primary sources (Fu et al., 2017). Hence, secondary sources of

copper will increasingly play a major role in copper supply. Sources of untapped waste copper, such as cattle footbaths, could be targeted as sources for recycled copper, providing farmers with a much-needed source of income and reduced waste burden. However, the recovery of copper from cattle footbaths via any method has not been explored to date.

The EU Water Framework Directive 2000/60/EC (WFD) (European Community, 2000) aims to deliver integrated river basin management for the whole of Europe. A key component of the Directive are the ecological targets for surface waters. Copper and zinc form part of the List II Group of metals which have a deleterious effect on the aquatic environment, and are subject to reduction programmes according to Directive 2006/11/EC on pollution caused by certain dangerous substances discharged into the aquatic environment (European Community, 2006). Heavy metals are non-biodegradable and can accumulate in living organisms (Fu and Wang, 2011). Some heavy metal ions are known to be toxic and carcinogenic, and are of particular concern in wastewater treatment (Burakov et al., 2018). Approaches to heavy metal removal in wastewater are flotation (Feng et al., 2017a, b, 2018) and chemical precipitation (Rojas, 2014). Greatly influencing the solubility of heavy metal hydroxides is pH where more basic pH leads to a reduction in solubility, which can then be removed via sedimentation (Hamid et al., 2016). However, this results in large quantities of low density, highly hydrated sludge, which has subsequent disposal issues (Fu and Wang, 2011). Adsorption is an economically and technologically viable method of removing heavy metals from wastewaters (Ali et al., 2018), particularly for low density sludge with low pH values (González et al., 2015). Layered double hydroxides (LDHs) are emerging as an effective absorbent for wastewater treatment due to their low cost, simple preparation, and high sorption efficiency, while extending the opportunity for waste valorisation (Liang et al., 2013). LDHs are known as hydrotalcite-like compounds or anionic clays, containing positively charged layers and exchangeable anions in the interlayer (Chen and Song, 2013). They consist of brucite-like layers, with a partial M^{II} for M^{III} substitution, leading to an excess of positive charge, compensated with anions situated in the interlayer, together with water molecules (Pérez et al., 2006). LDHs can be used as scavengers of dyes (Mohamed et al., 2018), phosphates (Li et al., 2016), oxoanions (Goh et al., 2008), heavy metals (Asiabi et al., 2017), and phenols and pesticides (Choy et al., 2007). This is due to their anion exchange, acid base and adsorption capability, with LDHs removing heavy metals via chemical precipitation and chelation (Liang et al., 2013). Chemical precipitation occurs due to localised pH buffering effects from the high concentration of OH^- (Park et al., 2007). LDHs have been shown to be an effective solid matrix for immobilising metals without substantially altering the environmental pH (González et al., 2015). The majority of studies exploring the potential of LDHs to recover copper have used Mg-Al LDHs for copper (Cu^{2+}) adsorption from simulated wastewater, with Cu^{2+} uptake between 20 and 181 mg g^{-1} in the literature (Anirudhan and Suchithra, 2008; Gong et al., 2011; González et al., 2015; Huang et al., 2015; Li et al., 2017; Ma et al., 2014, 2016; Yang et al., 2016; Yue et al., 2016). Higher levels of Cu^{2+} uptake have been reported for Zn-Al LDHs (450 mg g^{-1} (Chen and Song, 2013)) and for Ca-Al LDHs (381 mg g^{-1} (Rojas, 2014)). Ca-Al LDHs are usually used in cement fastening (Raki et al., 2004) and anion adsorption (Ghosal and Gupta, 2015), but demonstrated have high removal capacities and affinity for heavy metal ions (Rojas, 2014). Temperature is known to increase the uptake of copper for Mg-Al LDHs (Kameda et al., 2010), but the influence of temperature kinetics on Cu^{2+} uptake using Ca-Al LDHs has not been investigated.

This study explores the potential to remove copper from cattle footbaths and present the first successful investigation into the removal of copper and zinc from a commercially available cattle footbath powder mix solution. Isothermal and kinetic analysis of copper removal from a simulated wastewater was conducted using Ca_2-Al EDTA LDHs. Finally, the paper presents the real-world implications and applications of the

work, and how this can be applied to aide AMR metal resistance and co-selection mitigation in dairy farms.

2. Materials and methods

2.1. Cattle footbath and slurry preparation

Duplicate samples of used (6 h old) cattle footbath samples were collected from a high-performance dairy farm in the East Midlands of the UK. High copper content footbath powder (Hoof trimming limited, product code 0924: 25 kg to 200 L) is used on a weekly basis on the farm to protect against cattle lameness caused by bacterial infections. Cu^{2+}/Zn^{2+} footbaths were prepared according to manufacturer's instructions as follows; 25 kg was mixed with 200 L of water to give a 5% Cu^{2+} and Zn^{2+} solution. The footbath was stirred before collection and was sampled from different parts of the footbath. The used footbath samples were sterilized at 121 °C for 15 min. A 500 g portion of the same footbath powder was used for adsorption analysis experiments. The pH of the liquid samples was measured using a benchtop pH meter (HI5222, Hanna Instruments) with HI1131B glass body, double junction, combination pH electrode with HI7662-T temperature probe. Prior to taking the pH readings, the electrode was calibrated using buffers of pH 4.0, 7.01, and 10. After each reading the glass electrode was rinsed by deionised water before measuring the pH of the next sample.

2.2. Layered double hydroxide (LDH) synthesis and characterisation

In this study, two Ca-Al LDHs were formed for characterisation purposes; Ca_2Al-EDTA and Ca_2Al-NO_3. Ca-Al LDHs have historically formed with nitrate ion (NO_3^-) interlayer rather than carbonate (CO_3^{2-}) type (Raki et al., 2004). NO_3^- has been found to have the lowest affinity for the LDH layers in ion exchange compared with CO_3^{2-}, SO_4^{2-}, Cl^- (Bontchev et al., 2003; Châtelet et al., 1996). Due to this low affinity, the characterisation aimed to asses if the NO_3^- could be replaced by EDTA by adding sufficient quantities of EDTA during the synthesis process. Calcium-based LDHs exhibit a different crystal structure to other LDH materials, and preferentially form with nitrate ions in the interlayer rather than carbonate ions (Renaudin and François, 1999). LDH materials with Magnesium, and transition metals in the brucite like layers form preferentially with CO_3^{2-} ions, and as a result, are not as well suited to continuous synthesis with Na_2EDTA precursors (Pavlovic et al., 2009; Pérez et al., 2006). Continuous hydrothermal synthesis was carried out in the same counter–current flow reactor arrangement (Fig. 1) previously reported (Lester et al., 2012), with reaction conditions similar to those reported (Clark et al., 2017).

Briefly, a mixed metal salt solution containing $Ca(NO_3)_2 \cdot 4H_2O$ (0.067 M) and $Al(NO_3)_3 \cdot 9H_2O$ (0.033 M) was flowed up into the reactor at a rate of 10 mL min^{-1}, while the base (0.125 M NaOH) and Na_2EDTA (0.0167 M) solution was heated to 100 °C temperature in a 2 kW band heater and flowed down into the reactor at 20 mL min^{-1}. Pressure in the system was maintained at 15 MPa by a back-pressure regulator (Pressure Tech, UK). Following synthesis, samples were centrifuged, washed thoroughly and oven dried overnight at 70 °C.

Powder X-Ray Diffraction (XRD) analysis was completed using a Bruker D8-Advance diffractometer using Cu Kα radiation ($\lambda = 1.5418$ Å) in the 2θ range 5°–70° at a rate of 0.75° min^{-1}. XRD was used to establish LDH purity. The morphology of particles was elucidated with a Siemens XL30 (SEM) with an acceleration voltage of 20 kV. Nitrogen adsorption, using a Micromeritics Tristar II 3020 instrument at −196 °C, and the Brunauer-Emmett-Teller (BET) method were used to calculate surface area. Thermal stability was ascertained through thermogravimetric analysis (TGA) on a TA Q500 TGA instrument between 25 °C and 700 °C at a heating rate of 5 °C min^{-1} under N_2 flow at 40 mL min^{-1}. Fourier transform infra-red spectra were collected using a Bruker tensor FTIR ATR instrument between 500 and 1000 cm^{-1} and a resolution of 4 cm^{-1}.

2.3. Metal analysis

Multi-element analysis of diluted sterilized total footbath samples was undertaken by Inductively Coupled Plasma Mass Spectrometry (ICP-MS, iCAP-Q, Thermo Fisher Scientific) and individual element analysis of the experimental samples was undertaken using Atomic Absorption Spectrometry (AAS 272, Perkin Elmer). For ICP-MS analysis, the samples were first prepared via a total digestion method. 0.5 g liquid
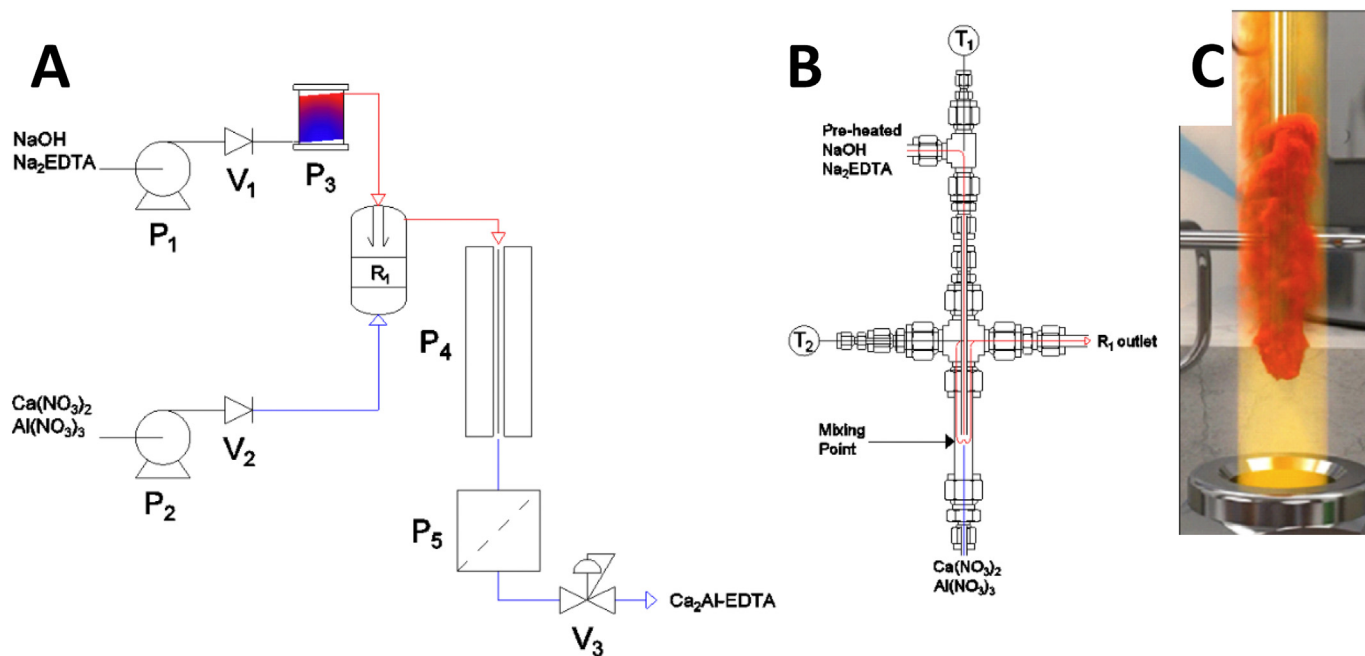

Fig. 1. A) Flow diagram of a continuous supercritical water reactor with animated depiction of nozzle reactor: P1 and P2 – Gilson HPLC pumps (P1 flow 20 mL min^{-1} P2 flow 10 mL min^{-1}), V1 and V2 – check valves, P3 2 kW band heater, R_1 counter current reactor, P4 heater exchanger, P_5 45 μm filter, V_3 Pressure Tech back pressure regulator. B) Schematic diagram of counter current reactor: T_1 and T_2 – Thermocouples. C) Animated depiction of reactor in operation.

and 0.2 g solid samples were mixed with 10 mL of concentrated nitric acid and then digested in a microwave digester (MARS X, CEM) at 190 °C, 38 Bar, for 45 min. Two milliliter of concentrated hydrochloric acid and 2 mL of concentrated hydrofluoric acid was added, and the digestion was repeated for 25 min. Thirty milliliter of boric acid was then added, and the digestion was repeated for 15 min. The digested samples were then diluted for analysis by ICP-MS. The ICP-MS was run employing three operational modes, including (i) a collision-cell (Q cell) using He with kinetic energy discrimination (He-cell) to remove polyatomic interferences, (ii) standard mode (STD) in which the collision cell is evacuated and (iii) hydrogen mode (H_2-cell) in which H_2 gas is used as the cell gas. Samples were introduced from an autosampler (Cetac ASX-520) incorporating an ASXpress™ rapid uptake module through a PEEK nebulizer (Burgener Mira Mist). Internal standards were introduced to the sample stream on a separate line via the ASXpress unit and included Ge (10 μg L^{-1}), Rh (10 μg L^{-1}) and Ir (5 μg L^{-1}) in 2% trace analysis grade (Fisher Scientific, UK) HNO_3. External multi-element calibration standards (Claritas-PPT grade CLMS-2 from SPEX Certiprep Inc.) included Ag, Al, As, Ba, Be, Cd, Ca, Co, Cr, Cs, Cu, Fe, K, Li, Mg, Mn, Mo, Na, Ni, P, Pb, Rb, S, Se, Sr, Tl, U, V and Zn, in the range 0–100 μg L^{-1} (0, 20, 40, 100 μg L^{-1}). A bespoke external multi-element calibration solution (PlasmaCAL, SCP Science) was used to create Ca, Mg, Na and K standards in the range 0–30 mg L^{-1}. Phosphorus, boron and sulphur calibration utilised in-house standard solutions (KH_2PO_4, K_2SO_4 and H_3BO_3). In-sample switching was used to measure B and P in STD mode, Se in H_2-cell mode and all other elements in He-cell mode. Peak dwell times were 10 mS for most elements with 150 scans per sample. Sample processing was undertaken using Qtegra™ software (Thermo-Fisher Scientific) utilising external cross-calibration between pulse-counting and analogue detector modes when required.

Copper and zinc levels of liquid solutions were measured using a Perkin Elmer AAS 272 atomic absorption spectrometer. An oxidising (lean blue) air-acetylene flame was used with 22 L min^{-1} air and 4 L min^{-1} acetylene flows with a 10 cm path length. Copper was measured on 4 wavelengths; 327.4 nm (10–60 mg L^{-1}) with 0.7 nm slit, 249.2 nm (60–300 mg L^{-1}) with 0.7 nm slit, 224.4 nm (100–1000 mg L^{-1}) with 0.2 nm slit, 244.2 nm (1000–6000 mg L^{-1}) with 0.7 nm slit. Zinc measured on 213.9 nm (0.1–2 mg L^{-1}) with 0.7 nm slit. Calibration curves were made from 1000 mg L^{-1} copper and zinc solutions (ROMIL PrimAg® element reference solutions) for sub 1000 mg L^{-1} analysis and 10,000 mg L^{-1} copper for analysis between 1000 and 10,000 mg L^{-1}.

2.4. Metal sorption studies

The adsorption experiments aimed to assess the potential of the LDH to adsorb copper from simulated copper solutions, and copper and zinc from the footbath powder solution used on the dairy farm. The first set of experiments used copper (II) sulphate pentahydrate ($Cu_2SO_4 \cdot 5H_2O$) ≥ 98% (Sigma-Aldrich) dissolved in deionised water as a simulated wastewater. The final set of experiments analysed the sorption of copper and zinc from cattle footbath solution made from the commercially sourced footbath powder mix (Section 2.1).

All solutions were prepared with deionised water (18 MΩ Milli Q, Millipore System). For all experiments, a 1 L aqueous solution $Cu_2SO_4 \cdot 5H_2O$ was prepared, and 200 ml was dispersed to 4 conical flasks. The flasks were placed in the incubator (Series 1A, LMS) and allowed to equilibrate for 1 h with constant stirring. Subsequently, 3 of the flasks had Ca_2Al-EDTA LDH sorbent added, while the fourth acted as a control. At specified intervals sample aliquots were taken, and then centrifuged. After centrifuging, the supernatants were quantitatively diluted and used to determine the metal levels with AAS (Section 2.4).

For the isotherm experiments, 0.05 g of Ca_2Al-EDTA LDH sorbent was added to 200 mL of aqueous $Cu_2SO_4 \cdot 5H_2O$ solution

(100–1000 mg L^{-1}). All isotherm experiments were conducted at 20 °C within the incubator. Samples were taken from the base solution ($t = 0$) and then after 60 min. The metal adsorbed per gram of sorbent (q_e) was calculated according to the equation:

$$q_e = \frac{(C_0 - C_e)V}{m} \tag{1}$$

where q_e (mg g^{-1}) is the equilibrium uptake, C_0 (mg L^{-1}) is the initial Cu^{2+} concentration, C_e (mg L^{-1}) is the Cu^{2+} concentration at equilibrium, V (mL) is the volume of adsorbate and m (g) is the mass of adsorbent.

2.5. Footbath waste adsorption studies

In order to establish industrial feasibility of the EDTA modified LDH for Cu^{2+} removal, the adsorbent was utilised in adsorption studies where the adsorbate was cattle footbath waste rather than a simulated wastewater solution of $Cu_2SO_4 \cdot 5H_2O$. The footbath wastewater was used both filtered and unfiltered to establish the effect of the suspended solids (TSS) on the adsorption capacity.

3. Results and discussion

3.1. Cattle footbath characterisation

Cattle footbaths have acidic pH values to ensure maximum solubility of the copper ions. The pH of the used footbath and fresh footbath solutions analysed in this study were 2.9 and 2.7 pH respectively, which is typical for solution containing heavy metal ions (Hashim et al., 2011) and prevents the precipitation of the copper hydroxide (Pavlovic et al., 2009). As manure accumulates in the footbath, due to the cows excreting as they walk through the footbath, the pH will increase, with the footbath becoming ineffective at a pH levels ≥ 4.5. Acidifiers such as sodium bisulphate are often added to the mix to safely the lower pH, thus increasing the solubility of the copper and extending its effectiveness. Fig. 2 shows that there are significant levels of sodium in the footbath (4879 mg L^{-1}), which is likely to be due to the Sodium Bisulphate. The ICP also shows that the copper (6184 mg L^{-1}) and zinc (8176 mg L^{-1}) are at the expected levels of around 5%. The ICP shows that the waste footbath also includes high levels of other elements, which may adsorb to the LDH sorbent. The adsorption of these metals were not examined during this study. The full ICP analysis can be found in the supplemental data, Table S1. The pH of the LDH powder in deionised water was 11.2, and the pH of the $Cu_2SO_4 \cdot 5H_2O$ solution was 5.7.

3.2. Structural characterisation of LDH materials

In order to establish if EDTA was present in the LDH after synthesis, Ca_2Al-NO_3 and Na_2EDTA were also characterised to allow for assessment of crystal structure and surface area changes. The XRD patterns of the Ca_2Al-EDTA and Ca_2Al-NO_3 (Fig. 3) show that EDTA modified Ca_2Al LDH exhibits some NO_3 intrusion into the interlayer region. The Ca_2Al-EDTA sample is also less crystalline than the Ca_2Al-NO_3 sample, with reflections at higher angles less defined than those in the NO_3 intercalated LDH. The lattice parameters for the Ca_2Al-NO_3 material are 0.6 nm and 1.7 nm for a and c respectively. However, for the Ca_2Al-ETDA LDH, there are multiple reflections at low Bragg angles, with reflections at 6.3° and 7.3°. The implication is that the reflections are both relating to EDTA in the interlayer region, but with different orientations (Rojas, 2014). Lattice parameters in the c plane relating to the reflections at 6.3° and 7.3° are 2.8 nm and 2.4 nm respectively.

The FTIR spectra for Ca_2Al-EDTA, Ca_2Al-NO_3 show broad absorption peaks between 3700 and 3000 cm^{-1}, relating to hydroxyl stretching in the metal hydroxide layers and hydrogen bonded water (Fig. 4).
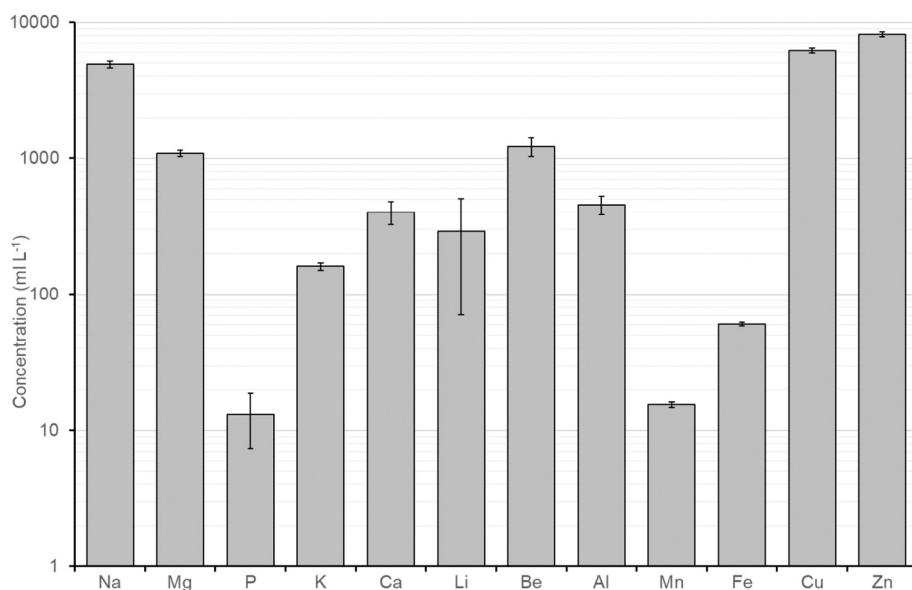
Fig. 2. ICP results for total waste cattle footbath. Full data set can be found in supplementary data Table S1. ($N = 3$).

The Ca_2Al-NO_3 sample also shows a strong absorption band 1400–1300 cm^{-1}, which corresponds to the nitrate in the interlayer region. The spectra also show a relatively high NO_3^- content in the Ca_2Al-EDTA sample, matching with the diffractograms. The absorption band between 1500 cm^{-1} and 1600 cm^{-1} represents the C=O bond in the CH_2—C=O part of the EDTA.

Fig. 5 shows SEM images of Ca_2AL-EDTA LDH formations. There is a clear formation of distinct hexagonal platelets with size 1–3 μm across hexagonal surface for Ca_2AL-EDTA (Fig. 5a) and 2–5 μm across hexagonal surface for Ca_2Al-NO_3 (Fig. 5b). Additionally, some larger clusters of agglomerated LDH have formed, but the hexagonal plate-shape morphology is still present. The smaller platelet size and more disordered structure to the agglomerates is attributed as cause of the increased surface area (S_{BET}) in Ca_2Al-EDTA when compared with Ca_2Al-NO_3. The S_{BET} for Ca_2Al-EDTA is 17.1 ± 0.1 m^2 g^{-1} and Ca_2Al-NO_3 is 5.5 m^2 g^{-1}. The TGA and DTA diagrams (Supplementary data, Fig. S1) exhibit the

typical thermal decomposition of LDH materials (Rojas, 2016). The first stage is the removal of surface (105 °C) and bound (225 °C) water, followed by dehydroxylation and decarbonation (up to 580 °C for Ca_2Al-NO_3 and 660 °C for Ca_2Al-EDTA). Thus, the LDH materials are thermally stable in the metal recovery temperatures of 10–40 °C.

3.3. Metal sorption studies

3.3.1. Adsorption isotherms

To establish if it was possible to recover Cu^{2+} from waste cattle footbaths, a scoping study was conducted using simulated wastewater with 200 mg L^{-1} $Cu_2SO_4 \cdot 5H_2O$ and 0.05 g of Ca_2Al-EDTA LDH. Fig. 6 shows the effect of contact time on the sorption capacity of Cu^{2+} ions by Ca_2Al-EDTA LDH. The majority of the sorption occurs rapidly within the process, and then stabilises to a much lower rate of adsorption, with equilibrium being reached after 45 min. For this scoping study,
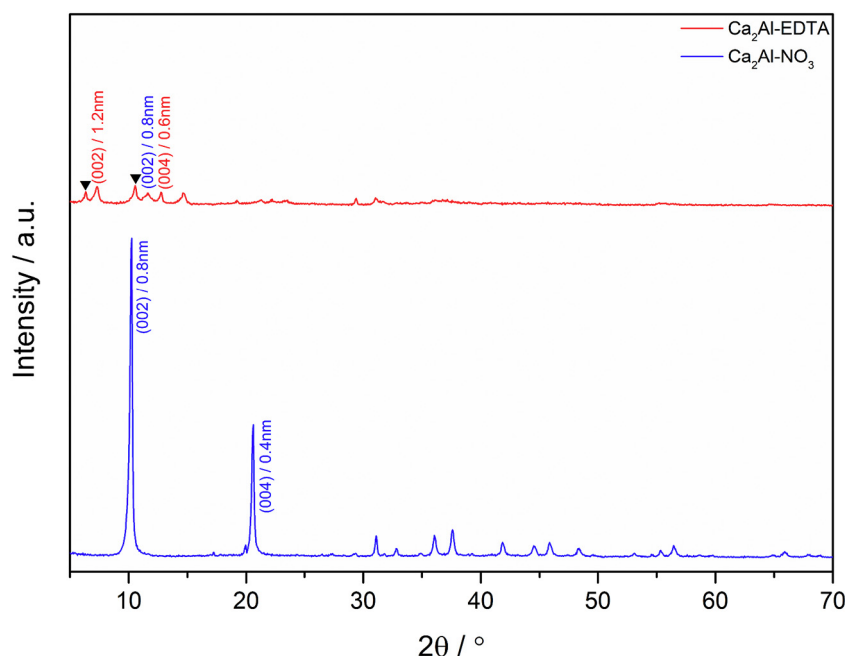

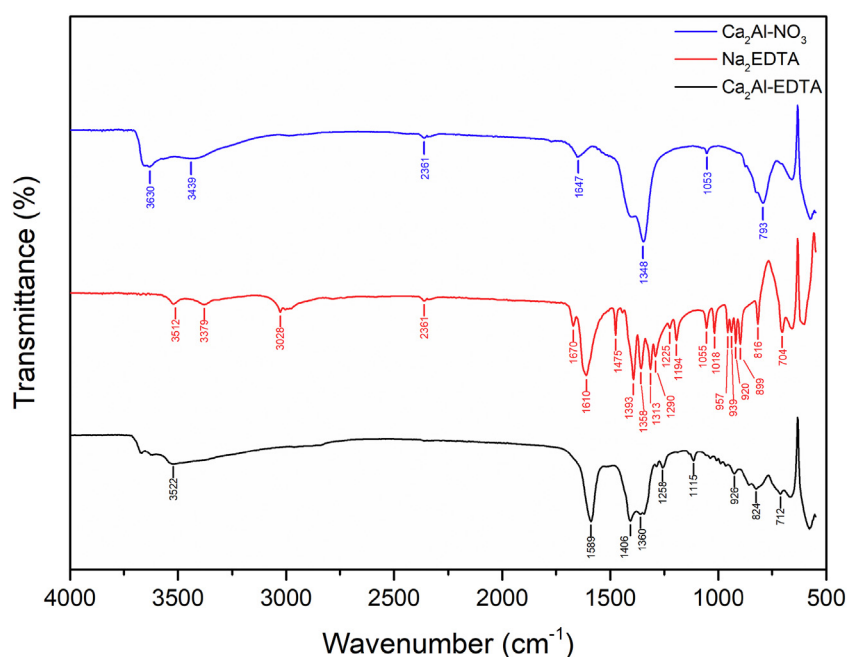**Fig. 3.** X-ray diffractograms of Ca_2Al-EDTA and a reference Ca_2Al-NO_3 sample.

Fig. 4. FTIR spectra for Ca$_2$Al-NO$_3$, Ca$_2$Al-EDTA, and Na$_2$EDTA.

56% (469 mg g^{-1}) of the Cu^{2+} ions were removed after 60 min. The final pH of the solution was 5.7, which is similar to previous studies (Huang et al., 2015).

The data from the adsorption studies was modelled according to the linear forms of the Langmuir (Eq. (2)) and Freundlich (Eq. (3)) isotherms:

$$\frac{C_e}{q_e} = \frac{C_e}{q_m} + \frac{1}{K_l q_m} \qquad (2)$$

where q_m is the maximum adsorption capacity of the LDH, K_l is the Langmuir constant.

$$\ln(q_e) = \ln(K_f) + \frac{1}{n}\ln(C_e) \qquad (3)$$

where K_f and n are Freundlich constants.

Fig. 7 shows the Cu^{2+} isotherm at 20 °C for Ca$_2$Al-EDTA LDH. The shape of the isotherm corresponds to a H type isotherm based on Giles Classification (Giles et al., 1960), and has a similar profile to that of a Cu^{2+} uptake isotherm previously reported (Rojas, 2014) for a Ca-Al LDHs. As Rojas noted, Ca-Al LDHs have a high affinity for Cu^{2+}, which is also higher than Mg-Al and Zn-Al LDHs for heavy metals. The application of the Langmuir (Eq. (2)) and Freundlich (Eq. (3)) isothermal equations to the experimental data (Table 1) show that the Langmuir model fitted most closely with the isothermal experimental data, with a regression coefficient (R^2) of 0.996. This means that the sorption process occurs in a monolayer, and that the distribution of active sites on the sorbent is homogeneous. The low 1/n value in the Freundlich model suggests a potential for heterogeneity within the material surface. This could be due to the fact that there are crystals where there is Ca$_2$Al-NO$_3$ and some crystals where there is Ca$_2$Al-EDTA. This would result in a difference in adsorption mechanics between the materials as there would be no intercalation where the NO$_3^-$ is intercalated. For this reason the Langmuir isotherm is focused on in the text. Based on the Langmuir model, the maximum theoretical Cu^{2+} uptake (q$_m$) is 568 mg g^{-1}. The affinity for copper uptake is significantly higher than that obtained for Mg-Al or Zn-Al LDHs (Zubair et al., 2017), and Ca-Al LDH (Rojas, 2014). As noted by Rojas, the precipitation mechanism, leading to the formation of the corresponding heavy metal hydroxides (Rojas, 2014), determined the removal behaviour due to the similar q$_e$ values at high C$_e$. Thus, the higher uptake of copper is due to the complexation of the copper in the EDTA interlayer, in addition to the precipitation mechanism.
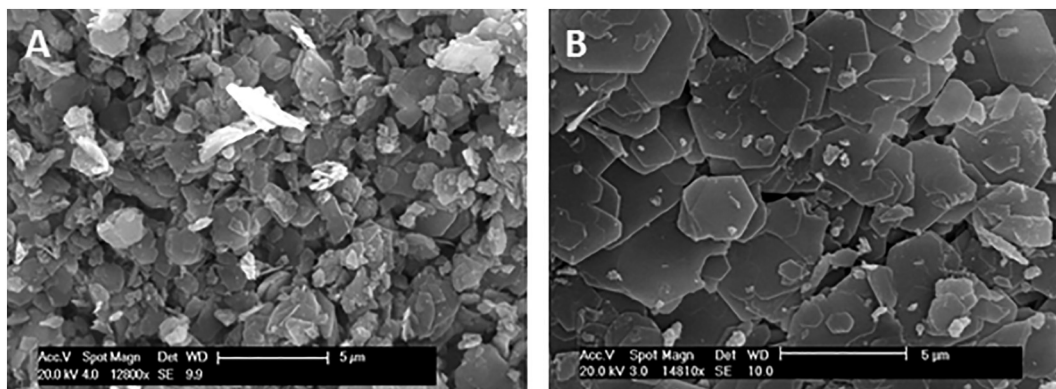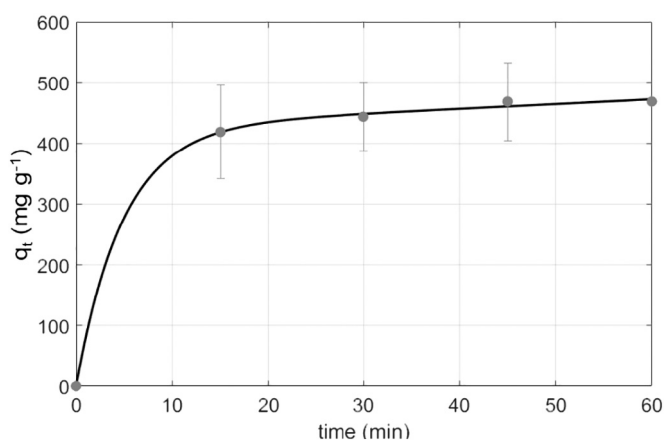

Fig. 5. SEM images of a) Ca$_2$Al-EDTA b) Ca$_2$Al-NO$_3$ LDH.

Fig. 6. Effect of contact time on sorption capacity (q_t) of Ca$_2$Al-EDTA LDH (0.05 g) for copper (II) sulphate pentahydrate solution at an initial concentration of 200 mg L^{-1}. N = 3 with error bars of standard deviation.

3.3.2. Sorption kinetics

In order to establish rates of adsorption; pseudo-first (Eq. (4)) and pseudo-second order (Eq. (5)) rate equations (Guo et al., 2013; Guzman-Vargas et al., 2016; Ni et al., 2007; Saiah et al., 2008; Sari and Tuzen, 2009) and the intra-particle diffusion model, developed by Weber and Morris (Doğan and Alkan, 2003; Guzman-Vargas et al., 2016), were applied to adsorption data. The pseudo-first order rate equation can be expressed in its linear form as (Guo et al., 2013):

$$\ln(q_e - q_t) = \ln(q_e) - k_1 t \tag{4}$$

where q_t is the Cu^{2+} uptake at a given time (mg g^{-1}), t is the given time (min) and k_1 (min^{-1}) is the pseudo-first order rate constant. The pseudo-second order rate equation can be expressed linearly as (Guo et al., 2013):

$$\frac{t}{q_t} = \frac{1}{k_2 q_e^2} + \frac{t}{q_e} \tag{5}$$

where k_2 is the pseudo-second order rate constant (g mg^{-1} min^{-1}). The intra-particle diffusion model can be presented as (Guzman-Vargas
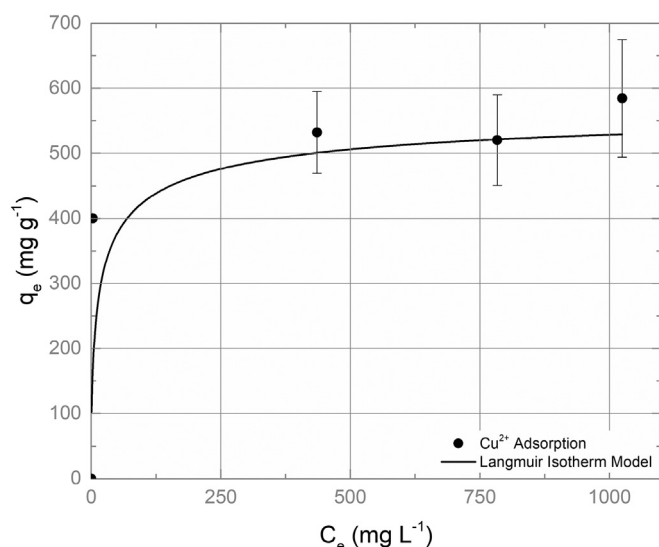

Fig. 7. Sorption isotherm of Cu^{2+} by Ca$_2$Al-EDTA LDH in the copper (II) sulphate pentahydrate solution. q_e is the equilibrium sorption capacity (mg g^{-1}), and C_e is the equilibrium concentration of metal ions in solution (mg L^{-1}). N = 3 with error bars of standard deviation.

Table 1
Langmuir and Freundlich parameters for the sorption of Cu^{2+} by Ca$_2$Al-EDTA LDH adsorbent in the copper (II) sulphate pentahydrate solution (N = 3).

	Langmuir equation			Freundlich equations		
	q_m (mg g^{-1})	k_l (L mg^{-1})	R^2	k_f mg g^{-1} (L mg^{-1})$^{1/n}$	$1/n$	R^2
Cu (II)	567.5	0.0580	0.996	375.2	0.0562	0.938

et al., 2016):

$$q_t = k_{id}\sqrt{t} + C \tag{6}$$

where k_{id} (mg g^{-1} min$^{-1/2}$) is the intra-particle diffusion rate constant. The kinetics of sorption describes the removal of Cu^{2+} ions by the LDH sorbents. In this study, the kinetics were analysed for Cu^{2+} removal from a 200 mg L^{-1} Cu^{2+} solution using Cu$_2$SO$_4$·5H$_2$O at 20 °C, 30 °C, and 40 °C. Fig. 8 shows the effect of contact time on the Cu^{2+} uptake in the presence of Ca$_2$Al-EDTA LDH at 20 °C, 30 °C, and 40 °C. There is a notable increase in uptake and rate of uptake as temperature increases. The most rapid increase in uptake during the first stage of sorption was for 40 °C (63% after 5 min) and reached equilibrium in the shortest time. The highest removal rate (498 mg g^{-1}) was also at 40 °C. The lowest final uptake was at 20 °C (427 mg g^{-1}). Previous studies for Cu^{2+} uptake with Mg-AL LDHS have taken between 2 and 24 h to equilibrate (González et al., 2015), which suggests that the rapid uptake and equilibrium of Ca$_2$Al-EDTA LDHs is due to a different uptake mechanism to Mg-AL LDHs.

The experimental kinetic data was fit to the pseudo-first-order (Eq. (4)), pseudo-second-order (Eq. (5)) as well as the Weber and Morris intra-particle diffusion (Eq. (6)) kinetic model equations, the parameters and linear regression coefficients (R^2) of which are presented in Table 2. Based on the correlation coefficient, the pseudo-second-order was the best fit for all the experimental data. This has been noted for several other similar studies for Mg-Al LDHs (González et al., 2015; Huang et al., 2015; Ma et al., 2014; Yang et al., 2016), but has not previously been noted for Cu^{2+} uptake kinetics of Ca-Al type LDHs. Additionally, the q_e values obtained via the pseudo-second-order model were similar to those obtained experimentally. This suggests that the pseudo-second-order model will work well for this LDH for the whole-time range. Thus, the second order sorption mechanism appears to be dominant, and the overall rate of metal uptake was controlled by a chemisorption process (Ho, 2006). The fit of the experimental data to the intra-particle diffusion model Eq. (6) provides an insight into the overall rate of sorption (Table 2). The intercept value (C) provides an indicator of the boundary layer thickness, with higher values representing a greater boundary layer effect. Table 2 shows that the intercept values obtained are much higher than those obtained in other studies (González et al., 2015), suggesting that intra-particle diffusion plays a strong role in the sorption process. Additionally, the high k_{ip} values indicate that there are many active sites on the surface of the Ca$_2$Al-EDTA LDH for Cu^{2+} ions to attach to, thus enhancing the diffusion rate.

3.3.3. Adsorption thermodynamics

The thermodynamic parameters of Gibbs free energy change $\Delta G°$, standard enthalpy $\Delta H°$, and standard entropy $\Delta S°$ of the kinetic data were also analysed to gain a greater insight into the effect of temperature on the adsorption. The thermodynamic parameters $\Delta G°$, $\Delta H°$, and $\Delta S°$ were calculated using the following equations:

$$\ln K_d = \frac{\Delta S^0}{R} - \frac{\Delta H}{RT} \tag{7}$$

$$K_d = \frac{q_e}{C_e} \tag{8}$$

where R is the ideal gas constant (8.314 kJ kmol^{-1} K^{-1}), T the temperature (K) and K_d the distribution coefficient. The plot of ln K_d against $1/T$
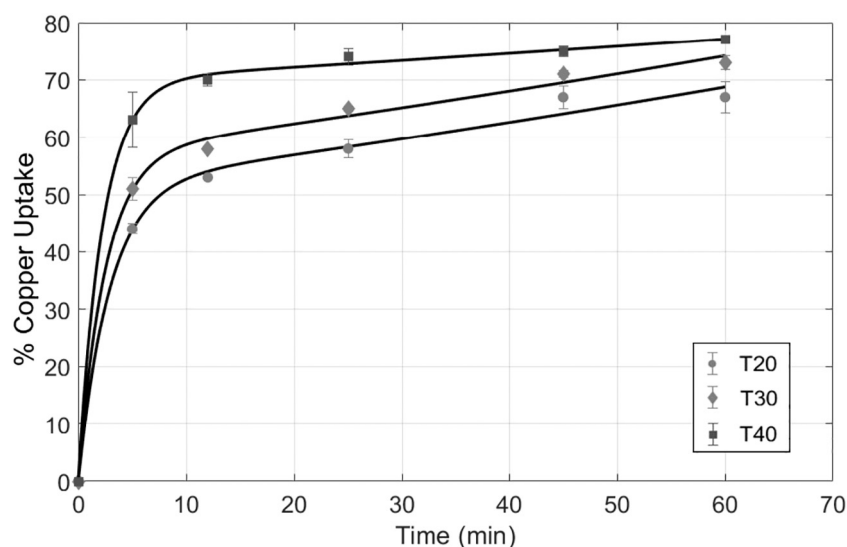
Fig. 8. Effect of contact time on % uptake of Cu^{2+} in the presence of Ca_2Al-EDTA LDH in a copper (II) sulphate pentahydrate solution at 20 °C, 30 °C, and 40 °C for conventional heating. Exponential lines of best fit are indicated for each temperature. $N = 3$ with error bars of standard deviation.

gives a straight line (Fig. 9); the slope and the intercept correspond to $\Delta H°/R$ and $\Delta S°/R$, respectively (Zaghouane-Boudiaf et al., 2012). $\Delta G°$ values at different temperatures used in experiments are calculated using the following equation:

$$\Delta G^0 = \Delta H^0 - T\Delta S^0 \qquad (9)$$

The thermodynamic parameters obtained from the analysis are presented in Table 3. The negative values of $\Delta G°$ at different temperatures indicate a thermodynamically favourable process due to the spontaneous nature of the adsorption. The change of free energy for chemisorption is a range of −80 to 400 kJ mol^{-1} (González et al., 2015). The $\Delta G°$ were between −6.18 and −4.55 kJ mol^{-1}, which indicates that the nature of adsorption was spontaneous and confirmed the affinity of material for Cu^{2+}. These values were in the middle of physisorption and chemisorption, and thus the process was a physical adsorption enhanced by a chemical effect. The decreasing values of $\Delta G°$ with increasing temperature suggest that the process increases in spontaneity at higher temperature. The positive $\Delta H°$ (19.3 kJ mol^{-1}) shows that the adsorption process was endothermic, and the positive $\Delta S°$ (81.3 kJ mol^{-1}) of the system indicates an increase in the randomness at the interface adsorbent/adsorbate during adsorption.

3.4. Potential for metal recovery from cattle footbath waste

While removing metal from simulated wastewater shows the potential for wastewater treatment using adsorbents, it is only by testing the adsorbents on real world wastewaters that the true capacity of LDH adsorbents can be explored. For Cu^{2+} removal from a commercial footbath solution, the kinetics were analysed at 20 °C in an incubator

from filtered and unfiltered 200 Cu^{2+} mg L^{-1} cattle footbath mix solutions. The aim was to analyse if the sediment inhibits copper uptake. For the filtered solution, the zinc concentration was also measured after treatment.

Fig. 8 shows the Cu^{2+} uptake for filtered and unfiltered footbath solutions and the Zn^{2+} uptake for the filtered footbath. Overall the percentage Cu^{2+} uptake is lower (filtered 50% and unfiltered 49% - Fig. 10) than that of the simulated wastewater (67%) after 60 min (Fig. 6). However, the uptake did not fully reach equilibrium within this time, and thus there is potential that the final uptake could be higher. The final uptake was 283 ± 11 mg g^{-1} filtered and 279 ± 22 mg g^{-1} unfiltered, which was lower than that of the simulated $Cu^2$$^+$ only wastewater (568 mg g^{-1}). However, the pH of the footbath solution (3.92) was lower than that of the simulated wastewater (4.97). In aqueous solutions, Cu^{2+} has been shown to be the dominant species at pH below 6 (Li et al., 2017), and Gong et al. (2011) found that solutions with an initial pH below 4 showed low initial uptake due to partial dissolution of the sorbent by acidic hydrolysis. Thus, the lower initial uptake could be related to the lower pH of the footbath solution, indicating that pH control is crucial to optimising the solution. No dissolution was experienced due to pH in this study. In addition to pH, the other elements and compounds within the footbath mix (Fig. 2) could be interfering with the sorption of the copper by occupying active sites on the LDH surface. It is important to note that the copper used in the footbath would be of a lower grade than the reagent grade (>98% purity) used for the simulated portion of this study. There is still a high initial uptake of copper (34% for filtered footbath) but is lower than the 44% uptake for the simulated wastewater. There is also the potential for competition for the same sorption sites, which has previously been noted for multi-component solutions and Ca-Al LDHs (Rojas, 2014).

Table 2
Maximum experimental adsorption capacity ($q_{e\ Exp}$), Coefficients of pseudo first-order, pseudo-second order, and intra-diffusion model for sorption of Cu^{2+} for 20 °C, 30 °C, and 40 °C from a copper (II) sulphate pentahydrate solution, and Cu^{2+} and Zn^{2+} uptake for footbath solutions on Ca_2Al-EDTA LDH ($N = 3$).

| Condition	$q_{e\ Exp}$ (mg g^{-1})	Pseudo first-order model			Pseudo second-order model			Intra-particle diffusion model		
		k_1 (min^{-1})	q_e (mg g^{-1})	R^2	k_2 (g mg^{-1} min^{-1})	q_e (mg g^{-1})	R^2	k_{ip} (mg g^{-1} $min^{-0.5}$)	C	R^2
Copper (II) sulphate pentahydrate solution Cu^{2+} 20 °C	427	0.0382	141.9	0.903	0.000604	446.6	0.998	23.7	248.5	0.972
Copper (II) sulphate pentahydrate solution Cu^{2+} 30 °C	493	0.0554	167.7	0.955	0.000660	515.5	0.999	24.8	312.9	0.963
Copper (II) sulphate pentahydrate solution Cu^{2+} 40 °C	498	0.0594	92.9	0.964	0.001482	509.4	1.000	14.5	395.9	0.896
Filtered footbath Cu^{2+} 20 °C	283	0.0396	93.9	0.892	0.000863	294.1	0.998	16.7	156.4	0.963
Unfiltered footbath Cu^{2+} 20 °C	274	0.0348	124.0	0.778	0.000523	294.1	0.994	21.5	110.8	0.985
Filtered footbath Zn^{2+} 20 °C	60	0.0005	0	0.029	0.001835	65.8	0.919	6.1	16.4	0.509
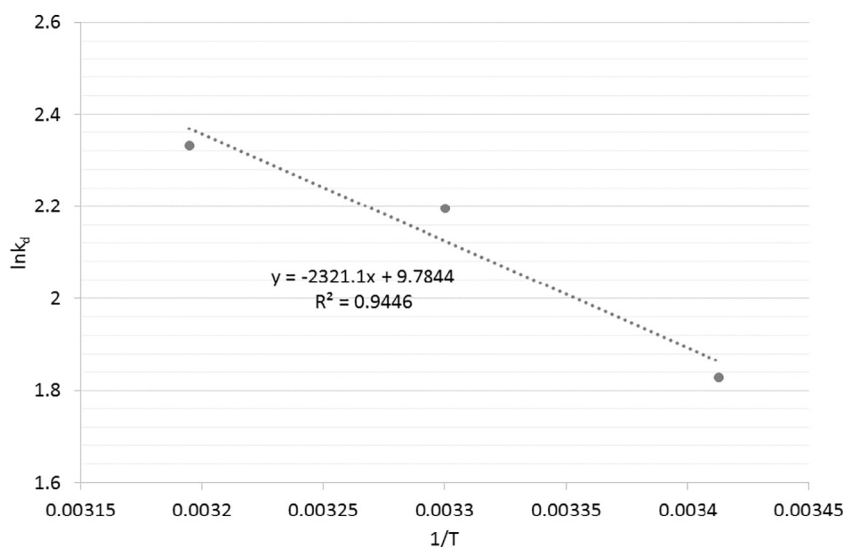
Fig. 9. Van't Hoff plot for the adsorption of Cu^{2+} on to Ca_2-Al EDTA LDHs in the copper (II) sulphate pentahydrate solution ($N = 3$).

As with the simulated wastewater study, the kinetic analysis showed that the pseudo second order model fits best with the Cu^{2+} experimental data ($R^2 = 0.998$ filtered, $R^2 = 0.994$ unfiltered), with q_e experimentally being close to that obtained with the model (Table 2). This shows that the pseudo-second-order model is applicable to single and multicomponent solutions for this sorbent, and that chemisorption processes also dominate the uptake mechanisms. The fit of the Zn^{2+} experimental data was poorer, but the pseudo-second-order model still fitted well ($R^2 = 0.919$), with q_e experimentally once more being close to that obtained with the model. While the uptake values of Zn^{2+} were low (60 mg g^{-1}) compared to Cu^{2+} (283 mg g^{-1}), they are still relatively high compared to the reported uptake of multiple metals on Mg-Al LDHs (Zubair et al., 2017), which use reagent grade metal solutions. The results imply that there is a stronger affinity for Cu^{2+} over Zn^{2+}, which has also been noted for Pb^{2+} and Cd^{2+} for other LDHs (González et al., 2014, 2015). Furthermore, the ICP data (Fig. 2) showed that several other metals were present in the footbath. Their removal potential was not investigated in this study as the focus was on the AMR metals of zinc and copper. However, the potential and affinity of LDHs to remove all of these metals requires further investigation.

The results demonstrate for the first time that it is possible to remove Cu^{2+} and Zn^{2+} ions from commercially available acidic pH cattle footbath solution using LDH adsorbents. Thus, these adsorbents could be used as heavy metal scavengers for low pH wastewaters with high pollutant concentrations. Research on novel sorbent materials rarely includes an assessment of scale up potential. Large scale manufacture of sorbent materials is required for them to be a feasible alternative to granular activated carbon, which is currently used at industrial scale. The LDHs used in this study were produced at gram scale using a laboratory scale counter–current flow reactor (Clark et al., 2017) and now at pilot and full scale (Clark et al., 2018). To date, few systems have been demonstrated in literature at larger scales (Dunne et al., 2015). Large scale continuous synthesis of LDHs is a relatively uncommon field, and only in batch systems (Dunne et al., 2018). However the continuous hydrothermal synthesis of LDHs and organic-modified LDHs utilises the same reactor design as some other continuously produced nanomaterials, which has been demonstrated on large scale (Caramazana-González et al., 2017; Caramazana et al., 2018; Dunne et al., 2016a, b; Lester et al., 2018; Munn et al., 2015).

It is known that high levels of copper and zinc in slurry wastewater disposed to land can lead to high levels of the metals in soil and crops (Jondreville et al., 2003). Given the potential for AMR metal resistance and co-selection due to bacterial exposure to high metal concentrations (Guo et al., 2018), there is a need to review the standard method of disposing of cattle footbath into farm slurry tanks. Currently there are no specific policy requirements which control the amount of footbath waste which can be disposed of in slurry tanks, or any limits on the duration the footbath waste can be stored before being spread on to the land. Further work is required to explore the influence of footbath solutions on AMR in slurry tanks. Furthermore, the results of this study fit with the objectives of the EU circular economy action plan (European Community, 2015) to boost the market for secondary raw material and water reuse. Given that there is the potential for up to 400 million L of waste cattle footbath to be used annually in the UK, the use of these footbaths is a considerable cost to farmers which could be mitigated by recovering and reusing the metals in the spent footbath solution, as well as being a large secondary source of copper and zinc sulphate. Thus, copper and zinc recovery from cattle footbath
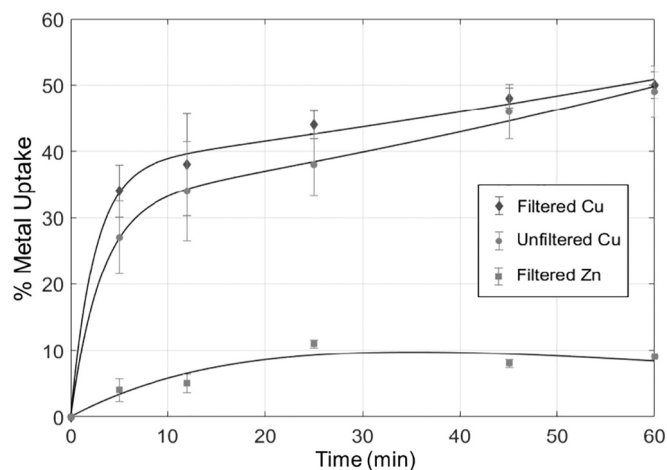
Table 3
Thermodynamic parameters for adsorption of Cu^{2+} on to Ca_2-Al EDTA LDHs in the copper (II) sulphate pentahydrate solution.

Temperature (K)	$\Delta G°$ (kJ mol^{-1})	$\Delta H°$ (kJ mol^{-1})	$\Delta S°$ (kJ mol^{-1} K^{-1})
293	−4.55	19.30	81.3
303	−5.36		
313	−6.18		

Fig. 10. Effect of contact time on % uptake of Cu^{2+} and Zn^{2+} from a 200 mg L^{-1} cattle footbath mix in the presence of Ca_2Al-EDTA LDH at 20 °C. Exponential lines of best fit are indicated for metal uptake. $N = 3$ with error bars of standard deviation.

wastes could be a substantial business opportunity for the farming community.

4. Conclusions

This study assesses the potential to remove copper from cattle footbaths. Isothermal and kinetic analysis of copper removal from a simulated wastewater have been presented for Ca$_2$-Al EDTA LDHs. This paper presents the first successful investigation into the removal of copper and zinc from a commercially available cattle footbath powder mix solution.

The Ca$_2$-Al EDTA LDHs used in this study removed a substantial amount of Cu^{2+} from a Cu$_2$SO$_4$·5H$_2$0 solution (568 mg g^{-1}). Increasing the temperature of the solution resulted in accelerated uptake, with higher equilibrium uptake reached in a shorted time. The pseudo-second-order model was found to be the most appropriate to describe the kinetics for both single and multi-component solutions investigated for the Ca$_2$Al-EDTA LDHs. Thus, the overall rate of metal uptake is controlled by chemisorption processes. The study showed for the first time that it is possible to adsorb Cu^{2+} and Zn^{2+} from a commercially available cattle footbath solution using adsorbents. While the uptake rate and final equilibrium value were lower than that of the single component solution, the uptake was higher than those recorded in literature for Mg-Al LDHs (filtered footbath solution Cu^{2+} uptake 283 mg g^{-1}, Zn^{2+} uptake 60 mg g^{-1}).

The study has shown that Ca$_2$Al-EDTA LDHs have the potential to effectively remove large quantities of copper and zinc from cattle footbath solutions without having to alter the environmental pH of the solution. Given that potentially nearly 400 million L of cattle footbath waste being disposed of annual into slurry tanks in the UK alone, there is a significant opportunity to access a valuable copper and zinc waste stream for secondary copper production, as well as remove a potential route of AMR co-selection and metal resistance on dairy farms.

Acknowledgements

Appendix A. Supplementary data

Supplementary data to this article can be found online at https://doi.org/10.1016/j.scitotenv.2018.11.330.

References

Ali, A., Gul, A., Mannan, A., Zia, M., 2018. Efficient metal adsorption and microbial reduction from Rawal Lake wastewater using metal nanoparticle coated cotton. Sci. Total Environ. 639, 26–39.

Anirudhan, T.S., Suchithra, P.S., 2008. Synthesis and characterization of tannin-immobilized hydrotalcite as a potential adsorbent of heavy metal ions in effluent treatments. Appl. Clay Sci. 42, 214–223.

Asiabi, H., Yamini, Y., Shamsayei, M., Tahmasebi, E., 2017. Highly selective and efficient removal and extraction of heavy metals by layered double hydroxides intercalated with the diphenylamine-4-sulfonate: a comparative study. Chem. Eng. J. 323, 212–223.

Baker, M., Hobman, J.L., Dodd, C.E.R., Ramsden, S.J., Stekel, D.J., 2016. Mathematical modelling of antimicrobial resistance in agricultural waste highlights importance of gene transfer rate. FEMS Microbiol. Ecol. 92, 1–10.

Bate, A., 2016. UK Dairy Industry Statistics. House Commons Libr.

Bontchev, R.P., Liu, S., Krumhansl, J.L., Voigt, J., Nenoff, T.M., 2003. Synthesis, characterization, and ion exchange properties of hydrotalcite Mg6Al2 (OH) 16 (A) x (A ') 2-x⊙ 4H2O (A, A ' = Cl-, Br-, I-, and NO3-, 2 ≥ x ≥ 0) derivatives. Chem. Mater. 2, 3669–3675.

Burakov, A.E., Galunin, E.V., Burakova, I.V., Kucherova, A.E., Agarwal, S., Tkachev, A.G., Gupta, V.K., 2018. Adsorption of heavy metals on conventional and nanostructured materials for wastewater treatment purposes: a review. Ecotoxicol. Environ. Saf. 148, 702–712.

Caramazana, P., Dunne, P., Gimeno-Fabra, M., McKechnie, J., Lester, E., 2018. A review of the environmental impact of nanomaterial synthesis using continuous flow hydrothermal synthesis. Curr. Opin. Green Sustain. Chem. 12, 57–62.

Caramazana-González, P., Dunne, P.W., Gimeno-Fabra, M., Zilka, M., Ticha, M., Stieberova, B., Freiberg, F., McKechnie, J., Lester, E.H., 2017. Assessing the life cycle environmental impacts of titania nanoparticle production by continuous flow solvo/hydrothermal syntheses. Green Chem. 19, 1536–1547.

Châtelet, L., Bottero, J.Y., Yvon, J., Bouchelaghem, A., 1996. Competition between monovalent and divalent anions for calcined and uncalcined hydrotalcite: anion exchange and adsorption sites. Colloids Surf. A Physicochem. Eng. Asp. 111, 167–175.

Chen, Y., Song, Y.F., 2013. Highly selective and efficient removal of Cr(VI) and Cu(II) by the chromotropic acid-intercalated Zn-Al layered double hydroxides. Ind. Eng. Chem. Res. 52, 4436–4442.

Choy, J.H., Choi, S.J., Oh, J.M., Park, T., 2007. Clay minerals and layered double hydroxides for novel biological applications. Appl. Clay Sci. 36, 122–132.

Clark, I., Dunne, P.W., Gomes, R.L., Lester, E., 2017. Continuous hydrothermal synthesis of Ca2 Al-NO3 layered double hydroxides: the impact of reactor temperature, pressure and NaOH concentration on crystal characteristics. J. Colloid Interface Sci. 504, 492–499.

Clark, I., Gomes, R.L., Crawshaw, C., Neve, L., Lodge, R., Fay, M., Winkler, C., Hull, M., Lester, E.H., 2018. Continuous synthesis of Zn2Al-CO3 Layered double hydroxides: a comparison of bench, pilot and industrial scale synthesis. React. Chem. Eng.

Department of Health, 2014. Antimicrobial Resistance (AMR) Systems Map.

Doğan, M., Alkan, M., 2003. Adsorption kinetics of methyl violet onto perlite. Chemosphere 50, 517–528.

Dunne, P.W., Munn, A.S., Starkey, C.L., Huddle, T.A., Lester, E.H., 2015. Continuous-flow hydrothermal synthesis for the production of inorganic nanomaterials. Philos. Trans. R. Soc. A Math. Phys. Eng. Sci. 373.

Dunne, P.W., Lester, E., Walton, R.I., 2016a. Towards scalable and controlled synthesis of metal-organic framework materials using continuous flow reactors. React. Chem. Eng. 1, 352–360.

Dunne, P.W., Starkey, C.L., Munn, A.S., Tang, S.V.Y., Luebben, O., Shvets, I., Ryder, A.G., Casamayou-Boucau, Y., Morrison, L., Lester, E.H., 2016b. Bench- and pilot-scale continuous-flow hydrothermal production of barium strontium titanate nanopowders. Chem. Eng. J. 289, 433–441.

Dunne, P.W., Lester, E., Starkey, C., Clark, I., Chen, Y., Munn, A.S., 2018. The chemistry of continuous hydrothermal/solvothermal synthesis of nanomaterials. In: Hunt, A.J., Attard, T.M. (Eds.), Supercritical and Other High-pressure Solvent Systems: For Extraction, Reaction and Material Processing. Royal Society of Chemistry, pp. 449–475.

European Community, 2000. Directive 2000/60/EC of the European Parliament and the Council of the European Union: Water Framework Directive, establishing a framework for community action in the field of water policy. Off. J. Eur. Commun L327 (43), 1–72. https://eur-lex.europa.eu/legal-content/EN/TXT/?uri=OJ:L:2000:327: TOC.

Community, European, 2006. Directive 2006/11/EC of the European Parliament and the Council of the European Union: pollution caused by certain dangerous substances discharged into the aquatic environment. Off. J. Eur. Union. L64 (49), 52–59. https://eur-lex.europa.eu/legal-content/EN/TXT/?uri=OJ:L:2006:064:TOC.

European Commission, 2015. Closing the loop - An EU action plan for the Circular Economy COM(2015), p. 614. https://eur-lex.europa.eu/legal-content/EN/TXT/?uri= CELEX%3A52015DC0614.

Feng, Q., Wen, S., Deng, J., Zhao, W., 2017a. Combined DFT and XPS investigation of enhanced adsorption of sulfide species onto cerussite by surface modification with chloride. Appl. Surf. Sci. 425, 8–15.

Feng, Q., Zhao, W., Wen, S., Cao, Q., 2017b. Activation mechanism of lead ions in cassiterite flotation with salicylhydroxamic acid as collector. Sep. Purif. Technol. 178, 193–199.

Feng, Q., Zhao, W., Wen, S., 2018. Surface modification of malachite with ethanediamine and its effect on sulfidization flotation. Appl. Surf. Sci. 436, 823–831.

Frenzel, M., Kullik, J., Reuter, M.A., Gutzmer, J., 2017. Raw material 'criticality'—sense or nonsense? J. Phys. D. Appl. Phys. 50, 123002.

Fu, F., Wang, Q., 2011. Removal of heavy metal ions from wastewaters: a review. J. Environ. Manag. 92, 407–418.

Fu, X., Ueland, S.M., Olivetti, E., 2017. Econometric modeling of recycled copper supply. Resour. Conserv. Recycl. 122, 219–226.

Ghosal, P.S., Gupta, A.K., 2015. An insight into thermodynamics of adsorptive removal of fluoride by calcined Ca-Al–(NO3) layered double hydroxide. RSC Adv. 5, 105889–105900.

Giles, C.H., MacEwan, T.H., Nakhwa, S.N., Smith, D., 1960. 786. Studies in adsorption. Part XI. A system of classification of solution adsorption isotherms, and its use in diagnosis of adsorption mechanisms and in measurement of specific surface areas of solids. J. Chem. Soc. 3973–3993.

Goh, K.H., Lim, T.T., Dong, Z., 2008. Application of layered double hydroxides for removal of oxyanions: a review. Water Res. 42, 1343–1368.

Gong, J., Liu, T., Wang, X., Hu, X., Zhang, L., 2011. Efficient Removal of Heavy Metal Ions From Aqueous Systems With the Assembly of Anisotropic Layered Double Hydroxide Nanocrystals @ Carbon Nanosphere. pp. 6181–6187.

González, M.A., Pavlovic, I., Rojas-Delgado, R., Barriga, C., 2014. Removal of Cu2+, Pb2+ and Cd2+ by layered double hydroxide-humate hybrid. Sorbate and sorbent comparative studies. Chem. Eng. J. 254, 605–611.

González, M.A., Pavlovic, I., Barriga, C., 2015. Cu(II), Pb(II) and Cd(II) sorption on different layered double hydroxides. A kinetic and thermodynamic study and competing factors. Chem. Eng. J. 269, 221–228.

Guo, Y., Zhu, Z., Qiu, Y., Zhao, J., 2013. Enhanced adsorption of acid brown 14 dye on calcined Mg/Fe layered double hydroxide with memory effect. Chem. Eng. J. 219, 69–77.

Guo, T., Lou, C., Zhai, W., Tang, X., Hashmi, M.Z., Murtaza, R., Li, Y., Liu, X., Xu, J., 2018. Increased occurrence of heavy metals, antibiotics and resistance genes in surface soil after long-term application of manure. Sci. Total Environ. 635, 995–1003.

Guzman-Vargas, A., Lima, E., Uriostegui-Ortega, G.A., Oliver-Tolentino, M.A., Rodriguez, E.E., 2016. Adsorption and subsequent partial photodegradation of methyl violet 2B on Cu/Al layered double hydroxides. Appl. Surf. Sci. 363, 372–380.

Hamid, H.A., Jenidi, Y., Thielemans, W., Somerfield, C., Gomes, R.L., 2016. Predicting the capability of carboxylated cellulose nanowhiskers for the remediation of copper from water using response surface methodology (RSM) and artificial neural network (ANN) models. Ind. Crop. Prod. 93, 108–120.

Hashim, M.A., Mukhopadhyay, S., Sahu, J.N., Sengupta, B., 2011. Remediation technologies for heavy metal contaminated groundwater. J. Environ. Manag. 92, 2355–2388.

Ho, Y.S., 2006. Review of second-order models for adsorption systems. J. Hazard. Mater. 136, 681–689.

Hobman, J.L., 2016. Antimicrobial metal ion resistance and its impact on co-selection of antibiotic resistance. Culture 36.

Hobman, J.L., Crossman, L.C., 2015. Bacterial antimicrobial metal ion resistance. J. Med. Microbiol. 64, 471–497.

Holzhauer, M., Bartels, C.J., Bergsten, C., van Riet, M.M.J., Frankena, K., Lam, T.J.G.M., 2012. The effect of an acidified, ionized copper sulphate solution on digital dermatitis in dairy cows. Vet. J. 193, 659–663.

Huang, G., Wang, D., Ma, S., Chen, J., Jiang, L., Wang, P., 2015. A new, low-cost adsorbent: preparation, characterization, and adsorption behavior of Pb(II) and Cu(II). J. Colloid Interface Sci. 445, 294–302.

Jondreville, C., Revy, P.S., Dourmad, J.Y., 2003. Dietary means to better control the environmental impact of copper and zinc by pigs from weaning to slaughter. Livest. Prod. Sci. 84, 147–156.

Kameda, T., Takeuchi, H., Yoshioka, T., 2010. Kinetics of uptake of Cu2+ and Cd2+ by Mg-Al layered double hydroxides intercalated with citrate, malate, and tartrate. Colloids Surf. A Physicochem. Eng. Asp. 355, 172–177.

Laven, R.A., Logue, D.N., 2006. Treatment strategies for digital dermatitis for the UK. Vet. J. 171, 79–88.

Lester, E., Aksomaityte, G., Li, J., Gomez, S., Gonzalez-Gonzalez, J., Poliakoff, M., 2012. Controlled continuous hydrothermal synthesis of cobalt oxide (Co3O4) nanoparticles. Prog. Cryst. Growth Charact. Mater. 58, 3–13.

Lester, E., Dunne, P., Chen, Y., Al-Atta, A., 2018. The engineering of continuous hydrothermal/solvothermal synthesis of nanomaterials. In: Hunt, A.J., Attard, T.M. (Eds.), Supercritical and Other High-Pressure Solvent Systems: For Extraction, Reaction and Material Processing. Royal Society of Chemistry, pp. 416–448.

Li, R., Wang, J.J., Zhou, B., Awasthi, M.K., Ali, A., Zhang, Z., Gaston, L.A., Lahori, A.H., Mahar, A., 2016. Enhancing phosphate adsorption by Mg/Al layered double hydroxide functionalized biochar with different Mg/Al ratios. Sci. Total Environ. 559, 121–129.

Li, Y., Bi, H.Y., Jin, Y.S., 2017. Facile preparation of rhamnolipid-layered double hydroxide nanocomposite for simultaneous adsorption of p-cresol and copper ions from water. Chem. Eng. J. 308, 78–88.

Liang, X., Zang, Y., Xu, Y., Tan, X., Hou, W., Wang, L., Sun, Y., 2013. Sorption of metal cations on layered double hydroxides. Colloids Surf. A Physicochem. Eng. Asp. 433, 122–131.

Ma, S., Chen, Q., Li, H., Wang, P., Islam, S.M., Gu, Q., Yang, X., Kanatzidis, M.G., 2014. Highly selective and efficient heavy metal capture with polysulfide intercalated layered double hydroxides. J. Mater. Chem. A 2, 10280.

Ma, L., Wang, Q., Islam, S.M., Liu, Y., Ma, S., Kanatzidis, M.G., 2016. Highly selective and efficient removal of heavy metals by layered double hydroxide intercalated with the MoS42-ion. J. Am. Chem. Soc. 138, 2858–2866.

Mohamed, F., Abukhadra, M.R., Shaban, M., 2018. Removal of safranin dye from water using polypyrrole nanofiber/Zn-Fe layered double hydroxide nanocomposite (Ppy NF/Zn-Fe LDH) of enhanced adsorption and photocatalytic properties. Sci. Total Environ. 640–641, 352–363.

Munn, A.S., Dunne, P.W., Tang, S.V.Y., Lester, E.H., 2015. Large-scale continuous hydrothermal production and activation of ZIF-8. Chem. Commun. 51, 12811–12814.

Ni, Z.M., Xia, S.J., Wang, L.G., Xing, F.F., Pan, G.X., 2007. Treatment of methyl orange by calcined layered double hydroxides in aqueous solution: adsorption property and kinetic studies. J. Colloid Interface Sci. 316, 284–291.

Northey, S., Mohr, S., Mudd, G.M., Weng, Z., Giurco, D., 2014. Modelling future copper ore grade decline based on a detailed assessment of copper resources and mining. Resour. Conserv. Recycl. 83, 190–201.

Pal, C., Asiani, K., Arya, S., Rensing, C., Stekel, D.J., Larsson, D.G.J., Hobman, J.L., 2017. Metal resistance and its association with antibiotic resistance. Adv. Microb. Physiol. 70, 261–313.

Park, M., Choi, C.L., Seo, Y.J., Yeo, S.K., Choi, J., Komarneni, S., Lee, J.H., 2007. Reactions of Cu2+ and Pb2+ with Mg/Al layered double hydroxide. Appl. Clay Sci. 37, 143–148.

Pavlovic, I., Pérez, M.R., Barriga, C., Ulibarri, M.A., 2009. Adsorption of Cu2+, Cd2+ and Pb2+ ions by layered double hydroxides intercalated with the chelating agents diethylenetriaminepentaacetate and meso-2,3-dimercaptosuccinate. Appl. Clay Sci. 43, 125–129.

Pérez, M.R., Pavlovic, I., Barriga, C., Cornejo, J., Hermosín, M.C., Ulibarri, M.A., 2006. Uptake of Cu2+, Cd2+ and Pb2+ on Zn-Al layered double hydroxide intercalated with edta. Appl. Clay Sci. 32, 245–251.

Raki, L., Beaudoin, J.J., Mitchell, L., 2004. Layered double hydroxide-like materials: nanocomposites for use in concrete. Cem. Concr. Res. 34, 1717–1724.

Renaudin, G., François, M., 1999. The lamellar double-hydroxide (LDH) compound with composition 3CaO·Al2O3·Ca(NO3)2·10H2O. Acta Crystallogr. Sect. C: Cryst. Struct. Commun. 55, 835–838.

Rojas, R., 2014. Copper, lead and cadmium removal by Ca Al layered double hydroxides. Appl. Clay Sci. 87, 254–259.

Rojas, R., 2016. Effect of particle size on copper removal by layered double hydroxides. Chem. Eng. J. 303, 331–337.

Saiah, F.B.D., Su, B.L., Bettahar, N., 2008. Removal of Evans blue by using nickel-iron layered double hydroxide (LDH) nanoparticles: effect of hydrothermal treatment temperature on textural properties and dye adsorption. Macromol. Symp. 273, 125–134.

Sari, A., Tuzen, M., 2009. Kinetic and equilibrium studies of biosorption of Pb(II) and Cd(II) from aqueous solution by macrofungus (amanita rubescens) biomass. J. Hazard. Mater. 164, 1004–1011.

Schmidt, M.G., Von Dessauer, B., Benavente, C., Benadof, D., Cifuentes, P., Elgueta, A., Duran, C., Navarrete, M.S., 2016. Copper surfaces are associated with significantly lower concentrations of bacteria on selected surfaces within a pediatric intensive care unit. Am. J. Infect. Control 44, 203–209.

Seiler, C., Berendonk, T.U., 2012. Heavy metal driven co-selection of antibiotic resistance in soil and water bodies impacted by agriculture and aquaculture. Front. Microbiol. 3, 1–10.

Summers, A.O., 2006. Genetic linkage and horizontal gene transfer, the roots of the antibiotic multi-resistance problem. Anim. Biotechnol. 17, 125–135.

Yang, F., Sun, S., Chen, X., Chang, Y., Zha, F., Lei, Z., 2016. Mg-Al layered double hydroxides modified clay adsorbents for efficient removal of Pb2+, Cu2+ and Ni2+ from water. Appl. Clay Sci. 123, 134–140.

Yu, Z., Gunn, L., Wall, P., Fanning, S., 2017. Antimicrobial resistance and its association with tolerance to heavy metals in agriculture production. Food Microbiol. 64, 23–32.

Yue, X., Liu, W., Chen, Z., Lin, Z., 2016. Simultaneous removal of Cu(II) and Cr(VI) by Mg–Al–Cl layered double hydroxide and mechanism insight. J. Environ. Sci. 1–11.

Zaghouane-Boudiaf, H., Boutahala, M., Arab, L., 2012. Removal of methyl orange from aqueous solution by uncalcined and calcined MgNiAl layered double hydroxides (LDHs). Chem. Eng. J. 187, 142–149.

Zhu, Y.-G., Johnson, T.A., Su, J.-Q., Qiao, M., Guo, G.-X., Stedtfeld, R.D., Hashsham, S.A., Tiedje, J.M., 2013. Diverse and abundant antibiotic resistance genes in Chinese swine farms. Proc. Natl. Acad. Sci. 110, 3435–3440.

Zubair, M., Daud, M., McKay, G., Shehzad, F., Al-Harthi, M.A., 2017. Recent progress in layered double hydroxides (LDH)-containing hybrids as adsorbents for water remediation. Appl. Clay Sci. 143, 279–292.